J Eng Math: (2022) 135:2
https://doi.org/10.1007/s10665-022-10218-7

On the lifetimes of two-dimensional droplets on smooth wetting patterns

Matthew Haynes · **Marc Pradas**

Received: 14 May 2021 / Accepted: 31 March 2022

Abstract We study the evolution and lifetime of droplets evaporating on a smooth chemical pattern, which is characterised by a spatially varying contact angle. We formulate a model that combines the evaporation rate of the droplet for a given volume with the static stability of the droplet as the volume changes in time quasi-statically. We derive an exact equation for the evaporation rate that is studied analytically under the limiting cases of nearly neutral wetting and highly hydrophilic conditions. We find that the evaporation rate of the droplet is highly dependent on the size and shape of the fictitious infinity where a far-field boundary conditions needs to be applied. We also study how the droplet's lifetime depends on the averaged contact angle and strength ε of the chemical pattern, observing that the lifetime of the droplet is maximised for a droplet with average contact angle $\pi/2$ and with $\varepsilon \lesssim 0.1$.

Keywords Evaporation rate · Sessile droplets · Wetting phenomena

1 Introduction

There has been a large amount of research devoted to understanding the motion of sessile droplets on solid surfaces. A key aspect of this problem is to quantify the effects of patterned surfaces on the droplet's motion. For the case of non-evaporating droplets see, e.g. [1–6], and for droplet evaporation process see, for example, [7–11]. The breadth of this research has been driven by the wide variety of real-life situations in which a sessile droplet can occur, as well as a large amount of industrial applications, such as for example, in the drying of integrated circuits [12], the spreading of metallic inks that are used in inkjet printing [13,14], or pattern deposition from particulates in a droplet [15,16].

In the absence of an external flow and temperature gradients, droplet evaporation is driven purely by diffusion. Under these conditions, the model of droplet evaporation must also describe the vapour transport from the droplet to the surrounding atmosphere [7]. The vapour profile surrounding a static droplet is harmonic and has direct

Grant No. EP/R041954/1.

M. Haynes · M. Pradas (✉)
School of Mathematics and Statistics, The Open University, Milton Keynes MK7 6AA, UK
e-mail: marc.pradas@open.ac.uk

M. Haynes
e-mail: haynes.matt@queensu.ca

Published online: 28 June 2022

similarities to other fields, such as for example electric potential fields in electrostatic studies [17], fluid flow in porous materials [18], and dissolution of bubbles [19,20]. There are many variables which influence the evaporation rate of the droplet. The relationship between the contact angle and the evaporation rate has been studied in the three-dimensional problem by making use of toroidal coordinates to study the lifetime of droplets under various conditions, for example in the stick-slip evaporation mode [21] or in the strongly hydrophobic limit [22]. These results have also been extended to include a surrounding shear flow [23].

In two dimensions, the difficulty occurs from the appropriate application of the far-field condition, i.e. that sufficiently far away from the droplet the presence of the droplet itself does not affect the vapour concentration. Indeed recently, an eloquent proof highlighted that in two dimensions, the far-field condition must be applied at a large but finite distance from the droplet to permit the existence of a solution [24]. To ensure that a solution exists, we shall impose a relaxed boundary condition following [25].

The classical understanding of droplet evaporation on a regular solid surface is that a droplet evaporates following a *stick-slip* model [26,27], also referred to as *stick-slide* [21,28], which has two phases – a *stick* phase and a *slide* phase that alternate from one another. During the *stick* phase, the droplet contact lines remain pinned to conserve the contact area and the contact angle decreases to accommodate the decreasing volume. In contrast, the *slide* phase conserves the contact angle while the contact line traverses. In addition, a second mode known as *stick-jump* has been recently reported, where intermittent contact line pinning causes the droplet to alternate between sticking and jumping [29–31]. It is generally well accepted that the emergence of stick-slip and stick-jump phenomena is a consequence of contact line pinning, which is itself a result of microscopic roughness or chemical defects of the solid surface, and hence generally difficult to control.

The study of droplet evaporation on smooth pinning-free surfaces has been sparked by the production of slippery surfaces, such as Slippery Liquid Infused Porous Surfaces [32–34] and Slippery Omniphobic Covalently Attached Liquid Like Surfaces [35]. These surfaces are characterised with a very low contact angle hysteresis and can be designed with topographical or wetting patterns [36]. The theory behind droplets atop smooth surface has been described in [37]. In addition, it has recently been shown that a droplet evaporating on a slippery surface that has a smooth macroscopic pattern follows a reproducible sequence of events that are characterised by bifurcations on the droplet's shape and position, and it has been referred to as *snap* evaporation, see [38] for topographical patterns and [39] for chemical patterns. In contrast to the stick-jump mode reported in [29], during snap evaporation, the droplet's contact line is never fully stationary but it moves very slowly except when a shape bifurcation occurs that forces the droplet to shift laterally and/or have a reduction of its base radius. In particular, the droplet may lose stability at certain critical values of its volume through snap-through and pitchfork bifurcations giving rise to dynamic snap events. A key assumption of this approach is a quasi-static evolution so that the state of the droplet is given by its equilibrium properties. Such approach has been used to quantify droplets evaporating on either smooth topographies [38] or chemical patterns [39], as well as for droplets with mass transfer moving on chemical patterns [40]. However, while all these works have focussed on the control of droplet motion on smooth patterns, little is known on the effect of patterning on the lifetime of evaporating droplets.

The primary focus of this paper is to investigate how the lifetime of the droplet is affected by the presence of a chemical smooth pattern, which is characterised by a spatially varying contact angle. Here, we propose a model that combines diffusion-limited evaporation with bifurcation theory. In particular, we formulate a framework which takes into account the evaporation rate of the droplet for a given shape while assuming that the shape and location of the droplet on the surface are dictated by the droplet's static stability as the volume changes in time. Importantly, we examine the stability from a quasi-static viewpoint and assume that the droplet moves from one stable solution to another significantly faster than any speed associated with the evaporation of the droplet. The full model yields an evolution equation for the droplet's volume which depends on the current configuration. Analysis of the evolution equation allows us to study both the evolution of the droplet and ultimately calculate the lifetime of the droplet for different wetting configurations.

This paper is organised as follows. In Sect. 2, we formulate the problem mathematically and define the key parameters of the system. Section 3 goes on to investigate the evaporation rate of a static droplet using a previously documented conformal mapping technique [25]. The evaporation rate is then tested against an asymptotic approx-

imation for a near neutral wetting droplet and the limiting case of a near vanishing contact angle [24]. Section 4 summarises the key results which are used to determine the stability of a droplet on a smooth patterned surface. The lifetime of a droplet is then examined in Sect. 5 by using the results from Sects. 3 and 4. We conclude in Sect. 6.

2 Problem formulation

Consider a two-dimensional droplet of liquid which has surface tension γ and density ρ at rest on a chemically patterned substrate. We define a Cartesian coordinate system, (x, y), with the x-axis running along the substrate and the y-axis normal to the surface. The droplet wets a region on the substrate which has half-width w and the centre of the droplet is located at $x = d$. In the absence of gravity, the equilibrium shape of the droplet is described by a circular segment with contact angle θ, and the volume of the droplet is given by

$$V = \frac{w^2}{2}\frac{2\theta - \sin 2\theta}{\sin^2\theta}. \tag{1}$$

We also assume that initially $d = 0$, i.e. the droplet is aligned with the centre of the coordinate system. Figure 1 shows a sketch of the droplet, where $\Theta(x)$ is the equilibrium contact angle imposed by the solid substrate.

We consider periodic chemical patterns that lead to a spatial variation of the equilibrium contact angle, $\Theta(x)$, of the form

$$\Theta(x) = \theta_0\left[1 + \varepsilon\cos(kx)\right], \tag{2}$$

where θ_0 is the average contact angle, ε is the ratio of the pattern's amplitude to its average contact angle, i.e. $\theta_0\varepsilon$ is the amplitude of the pattern, and $k = 2\pi/\lambda$, where λ is the wavelength of the pattern. Here, we assume that typical length scale λ is comparable to the droplet's footprint. To ensure that the contact angle has physical relevance, we impose the constraint $\Theta(x) < \pi$ everywhere and hence we find bounds for ε, i.e.

$$|\varepsilon| < \frac{\pi}{\theta_0} - 1. \tag{3}$$

Note that at equilibrium the contact angle of the droplet is given by $\theta = \Theta(d \pm w)$ with a volume given by Eq. (1). It is also important to remark, that while, in this paper, we focus on sinusoidal patterns, the methods presented here are applicable to any patterning that has an inherent length scale.

We model the evaporation of the droplet as a quasi-static, diffusion-limited process and assume that the surrounding fluid is stationary. The quasi-static condition here means that the evaporation time scale is assumed to be much slower than the droplet's relaxation time scale, so that we can use a semi-circular approximation for the

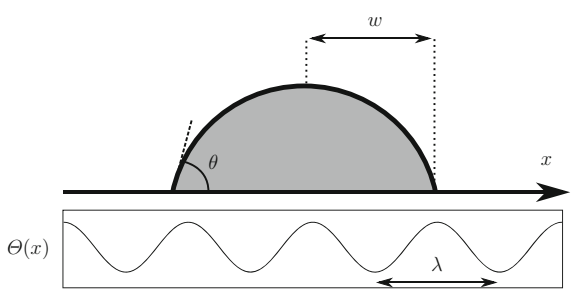

Fig. 1 A two-dimensional droplet resting on a flat solid surface with a smooth chemical pattern that is quantified in terms of the equilibrium contact angle $\Theta(x)$. The wavelength of the pattern is λ and the droplet's footprint is denoted by w. The circular shape of the droplet is quantified in terms of the contact angle θ, which is the same on both contact points

droplet's shape. The evaporation rate is found by calculating the mass flux of liquid vapour across the boundary of the droplet. To this end, we will find first the liquid vapour profile in the surrounding fluid (although we note that in general this is not always necessary [41]). Under these assumptions, the liquid vapour concentration, $c(x, y)$, is harmonic in the surrounding fluid and has a saturated value, c_{sat}, on the boundary of the droplet. In the far-field limit, the liquid vapour concentration has a constant value that we denote c_∞. To ensure that a solution exists, we apply the far-field condition on a finite curve [25]. Specifically, we enforce this condition on the perimeter of the upper-semi-circle with radius $R \gg w$. In summary, the concentration of liquid vapour satisfies

$$\nabla^2 c = 0 \ \text{ for } (x, y) \in \Omega \subset \mathbb{R}^2, \tag{4a}$$

$$c = c_{\text{sat}} \ \text{ on } y = h(x), \tag{4b}$$

$$c = c_\infty \ \text{ on } y = \sqrt{R^2 - x^2}, \tag{4c}$$

$$\frac{\partial c}{\partial y} = 0 \ \text{ on } y = 0,\ w < |x| < R, \tag{4d}$$

where Ω is the region of $\mathbb{R}^2$ bounded by the curves $y = 0$, $y = h(x)$ and $y = \sqrt{R^2 - x}$. Here, $y = h(x)$ describes the droplet's interface, and (4d) is the standard no flux boundary condition applied on the solid surface. From the liquid vapour profile in the surrounding fluid, the evaporation rate, i.e. the volume change rate, is then calculated through

$$\frac{\mathrm{d}V}{\mathrm{d}t} = D \int_{d-w}^{d+w} \left.\frac{\partial c}{\partial n}\right|_{y=h(x)} \sqrt{1 + \left(\frac{\mathrm{d}h}{\mathrm{d}x}\right)^2}\, \mathrm{d}x, \tag{5}$$

where n is a coordinate normal to the surface and D represents the diffusion coefficient. It is convenient to non-dimensionalise the system by defining the following variables:

$$(x, y) = \lambda(x^*, y^*), \qquad V = \lambda^2 V^*, \qquad c = c_\infty + (c_{\text{sat}} - c_\infty)c^*, \qquad t = \frac{\lambda}{D(c_{\text{sat}} - c_\infty)} t^*, \tag{6}$$

where λ is the wavelength of the patterning, i.e. $\lambda = 2\pi/k$, and the starred variables are all dimensionless. Henceforth, the stars will be dropped and all variables should be considered dimensionless, unless otherwise stated. With these new variables, the Laplace system (4) becomes

$$\nabla^2 c = 0 \ \text{ for } (x, y) \in \Omega \subset \mathbb{R}^2, \tag{7a}$$

$$c = 1 \ \text{ on } y = h(x), \tag{7b}$$

$$c = 0 \ \text{ on } y = \sqrt{R^2 - x^2}, \tag{7c}$$

$$\frac{\partial c}{\partial y} = 0 \ \text{ on } y = 0,\ w < |x| < R, \tag{7d}$$

and Eq. (5) for the evaporation rate becomes

$$\frac{\mathrm{d}V}{\mathrm{d}t} = \int_{d-w}^{d+w} \left.\frac{\partial c}{\partial n}\right|_{y=h(x)} \sqrt{1 + \left(\frac{\mathrm{d}h}{\mathrm{d}x}\right)^2}\, \mathrm{d}x. \tag{8}$$

In the following, we find an exact equation which gives the evaporation rate of a droplet for a given (dimensionless) width and contact angle. While in Sect. 4, we shall study the stability of a droplet for a given (dimensionless) volume

resting on a substrate with local contact angle given by (2). These results will allow us to form a first-order ordinary differential equation to describe the evolution of the droplet and hence determine its lifetime.

3 Evaporation rate

In the first part of this section, we summarise the work of [25], in which an exact equation for the droplet's evaporation rate is derived in terms of the droplets half-width, w, and contact angle, θ. We shall then investigate special cases where the evaporation rate can be written explicitly. We introduce the local inclination angle, $\phi \in [-\pi, \pi]$, which is defined as the angle formed against the horizontal, to describe the surface of the droplet as

$$x = -w\frac{\sin\phi}{\sin\theta}, \tag{9a}$$

$$h = -w\frac{\cos\theta - \cos\phi}{\sin\theta}. \tag{9b}$$

We note that this formulation is applicable for all contact angles, unlike a direct formulation using $h(x)$. Since the shape of the droplet is a circular segment, we use the conformal mapping

$$\frac{z-w}{z+w} = \left(\frac{\zeta - a}{\zeta + a}\right)^{\sigma}, \tag{10}$$

where $z = x + \mathrm{i}y$ is the complex variable in the physical plane, $\sigma = 2(1-\theta/\pi)$, $a = w/\sigma$, and ζ is the complex variable in the transformed plane, see Fig. 2.

We note that (10) maps the z-plane onto the ζ-plane, and in particular, a circular arc of width w and contact angle θ is mapped to the perimeter of the upper half circle with radius a. In the transformed space, we can solve the Laplace system (7) to find the complex potential, χ, (which satisfies $\mathrm{Re}(\chi) = c$) given by

$$\chi(\zeta) = 1 - \frac{\ln(\zeta/a)}{\ln(R/a)}. \tag{11}$$

Taking the derivative of χ with respect to z, we find the mass flux across the surface

$$\frac{\mathrm{d}\chi}{\mathrm{d}z} = -\frac{1}{\zeta\ln(R/a)}\frac{4a^2 g^{\frac{1-\sigma}{\sigma}}}{(z+w)^2(1-g^{\frac{1}{\sigma}})^2}, \tag{12}$$

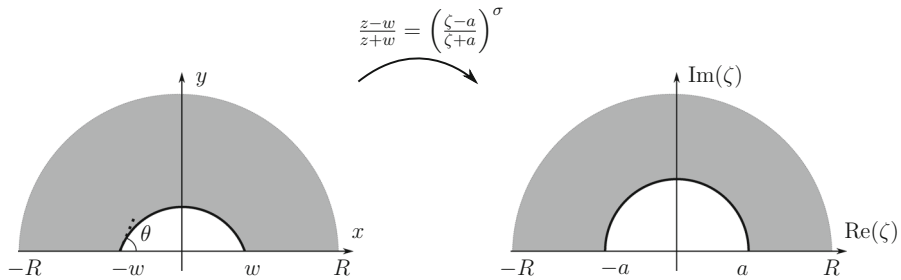

Fig. 2 Diagram showing how a circular segment with angle θ and width w is mapped to the upper semi-circle with radius $a = w/\sigma$ using (10), where $\sigma = 2(1-\theta/\pi)$. The grey shaded region in the left diagram is a depiction of Ω, and in the right diagram, it depicts the transformed domain

where $g(z) = (z - w)/(z + w)$. It follows that the normal derivative of the concentration is given by

$$\frac{\partial c}{\partial n} = \hat{\boldsymbol{n}}_x \mathrm{Re}\left(\frac{\mathrm{d}\chi}{\mathrm{d}z}\right) - \hat{\boldsymbol{n}}_y \mathrm{Im}\left(\frac{\mathrm{d}\chi}{\mathrm{d}z}\right), \tag{13}$$

where $\hat{\boldsymbol{n}}_x, \hat{\boldsymbol{n}}_y$ are the x, y components of the outward unit normal to the droplet's interface. Hence, we can use (13) to find the evaporation rate, (8), which, in these transformed coordinates, is given as

$$\frac{\mathrm{d}V}{\mathrm{d}t} = \frac{w}{\sin\theta}\int_{-\theta}^{\theta} \left.\frac{\partial c}{\partial n}\right|_{(x(\phi),h(\phi))} \mathrm{d}\phi, \tag{14}$$

with $x(\phi)$ and $h(\phi)$ given in (9). Equation (14) is the principle result of this section. It is an exact equation that predicts the evaporation rate of a droplet for a given width w and contact angle θ. In the following, we study two special cases for which it is possible to find asymptotic solutions of Eq. (14).

3.1 Limiting cases

We start by considering the case of nearly neutral wetting, i.e. the droplet interface is close to a semi-circle with the contact angle satisfying $|\theta - \pi/2| \ll 1$. Observe that the surface of the droplet is then described, in polar coordinates (r, φ), by

$$r = w(1 + \varepsilon \sin\varphi) + \mathcal{O}(\varepsilon^2), \tag{15}$$

where $\varepsilon = \theta - \pi/2$. We consider a regular expansion for the concentration in terms of ε. By solving the resulting leading and first-order systems, we find that the concentration is given by (see Appendix A for a derivation)

$$c = 1 - \frac{\ln\frac{r}{w}}{\ln\frac{R}{w}} + \varepsilon\left[\frac{2}{\pi\ln\frac{R}{w}}\left(1 - \frac{\ln\frac{r}{w}}{\ln\frac{R}{w}}\right) + \frac{4}{\pi\ln\frac{R}{w}}\sum_{n=1}^{\infty}\frac{\cos(2n\varphi)}{1-4n^2}\frac{\left(\frac{r}{R}\right)^{2n} - \left(\frac{R}{r}\right)^{2n}}{\left(\frac{w}{R}\right)^{2n} - \left(\frac{R}{w}\right)^{2n}}\right] + \mathcal{O}(\varepsilon^2). \tag{16}$$

By noting that the outward unit normal vector satisfies

$$\hat{\boldsymbol{n}} = \hat{\boldsymbol{r}} - (\varepsilon\cos\varphi)\hat{\boldsymbol{\varphi}} + \mathcal{O}(\varepsilon^2), \tag{17}$$

and applying Eq. (16) to (8) we find

$$\frac{\mathrm{d}V}{\mathrm{d}t} = -\frac{\pi}{\ln\frac{R}{w}} - \frac{2\varepsilon}{\left(\ln\frac{R}{w}\right)^2} + \mathcal{O}(\varepsilon^2), \tag{18}$$

which gives the evaporation rate of a nearly neutral wetting setting.

The second special case we consider is the extremely hydrophilic droplet, i.e. a droplet with asymptotically small contact angle. This case has been examined in [24], and here, we give a brief summary of that method.

In this method, the far-field condition is not applied on the boundary of a semi-circle; instead, an upper semi-ellipse is used. This choice of fictitious infinity is to allow a sufficiently tractable conformal mapping solution. Using the upper semi-ellipse with major-axis $\sqrt{R^2+1}$ that is aligned with the x-axis and minor-axis R as the fictitious infinity, i.e.

$$\left(\frac{x}{\sqrt{1+R^2}}\right)^2 + \left(\frac{y}{R}\right)^2 = 1, \tag{19}$$

we see that the domain is mapped to the rectangular domain $(u, v) \in (-1, 1) \times (0, S)$ by the conformal mapping

$$z = -w \sin\left(\frac{\pi}{2}\zeta\right), \tag{20}$$

where $\zeta = u + \mathrm{i}v$ and S satisfies $R = 2\sinh\left(\frac{\pi S}{w}\right)$. In the transformed space, we obtain the complex potential

$$\chi = 1 - \frac{v}{S} = 1 - \frac{\mathrm{Im}(\zeta)}{S}. \tag{21}$$

This result is then mapped back to the z-plane and applied to (8) to find

$$\left.\frac{\mathrm{d}V}{\mathrm{d}t}\right|_{\theta=0} = -\frac{\pi}{\mathrm{asinh}(R/w)}. \tag{22}$$

3.2 Numerical results for homogeneous surfaces

We present here numerical results of Eq. (14) for a given and constant contact angle. In particular, in this section, we examine the instantaneous evaporation rate for a defined droplet, while the examination of a droplet lifetime is discussed in Sect. 5. We note that to fully determine the solution of the droplet, we need to either fix the volume V of the droplet or its width w. We consider each of these two cases in turn.

We start by fixing the width of the droplet to $w = 1$. As we vary the contact angle, the droplet's volume is then given by Eq. (1). Figure 3a shows numerical results of Eq. (14) for different values of R. The blue and red lines represent the results from the asymptotic limiting cases given by Eq. (22) (nearly complete wetting) and (18) (nearly neutral wetting), respectively. We see that in both cases, there is excellent agreement between numerical and asymptotic results. We note that for the case of $\theta = 0$, the asymptotic result becomes more accurate as R increases (see inset panel of Fig. 3a). This is because in the analytical treatment of the zero contact angle case, the far-field conditions are applied on the elliptic curve (19) which tends to the circular arc of radius R as $R \to \infty$. We also see that the asymptotic results derived here for nearly neutral wetting meet the exact results at a tangent to the point $\theta = \pi/2$, as expected [24] .

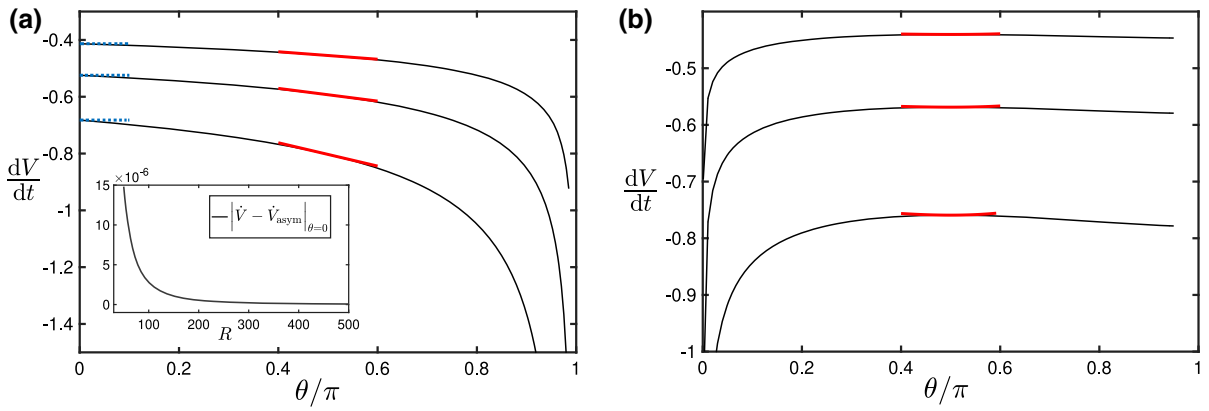

Fig. 3 Evaporation rates given by Eq. (14) with $w = 1$ (**a**) and $V = 1$ (**b**). The three curves correspond (from bottom to top) to $R = 50, 200, 1000$, respectively. Red lines in panels **a** and **b** correspond to the evaporation rates given by Eq. (18) (neutral wetting), and blue dashed lines in panel **a** are plots of Eq. (22) (complete wetting limit). The inset panel in **a** shows the difference between the numerical results from Eq. (14) and the asymptotic result (22) as a function of R. (Color figure online)

Figure 3b shows the evaporation rate as a function of the contact angle when the volume of the droplet is fixed. Under this condition, the droplet's width is given by

$$w = \sin\theta \left(\frac{2V}{2\theta - \sin 2\theta} \right)^{1/2}. \tag{23}$$

The red lines in Fig. 3b represent the asymptotic analysis given by Eq. (18), where we can see, again, that the two lines meet in tangent at $\theta = \pi/2$. In order to conserve the volume as $\theta \to 0$, we observe that $w \to +\infty$, and therefore, the extremely hydrophilic case, given by (22), predicts that the volume change rate tends to negative infinity. This agrees with the numerical results shown in Fig. 3b.

4 Stability analysis: bifurcation diagrams

As is discussed in Sect. 1, the evolution of a droplet evaporating under quasi-static conditions can be described by its equilibrium properties. As the droplet slowly evaporates the shape and location of the droplet can be modelled by studying the stability of the equilibrium solutions. This approach has recently been used to describe droplets evaporating on chemical patterns [39] and droplet with mass transfer moving on chemical patterns [40]. This section reviews the work presented in these references to study the static stability of a droplet with known volume on a smooth patterned surface. This analysis will be used later in our evolution model, where we assume that the droplet will only follow stable points. Further, we shall assume that the droplet moves between stable solutions instantaneously, as discussed in the introduction. It is important to emphasise that the process of droplet evaporation is an intrinsically dynamic situation, which in general would require a dynamic stability analysis. However, here we are assuming that the evaporation process is sufficiently slow (quasi-static) such that we can use static stability analysis to effectively predict the evolution of the droplet.

To ensure we have an equilibrium configuration the forces along the substrate must balance hence,

$$\Theta(d + w) = \Theta(d - w), \tag{24}$$

and we define this contact angle to be θ. This relation shows that for sinusoidal patterns the droplets centre aligns with a maximum or minimum of the patterning, or that the width of the droplet (i.e. $2w$) is a integer multiple of the pattern wavelength. It has been shown that only the droplets which align with a maximum or minimum of the patterning can be stable [39,40]. In addition, the stability of those solutions depend on the droplet's volume and solutions that are centred on a maximum or minimum of the patterning can be stable, partially stable (saddle node) or fully unstable. The term partially stable is used, in this context, to describe the stability to symmetric perturbations but unstable to asymmetric perturbations. Indeed, for small volumes or small ε all droplets aligned with a maximum or minimum of the patterning are stable to symmetric perturbations. As ε increases, solutions undergo a pitchfork bifurcation to lose their stability to symmetric perturbations [39].

The stability of a two-dimensional droplet can be determined from the interfacial energy, which in its dimensionless form is

$$E = \frac{2\theta w}{\sin\theta} - \int_{d-w}^{d+w} \cos\Theta(x)\,\mathrm{d}x, \tag{25}$$

where the first term of the RHS describes the contribution from the liquid/gas interface and the second term quantifies the solid/fluid interfacial contribution to the energy. In the above equation, θ is the contact angle that satisfies (24) and, for a given volume V, is related to the half-width w through Eq. (1). The stability of a given (V, d, w) triple is then found by numerically evaluating the Hessian matrix of the energy, and determining the number of positive

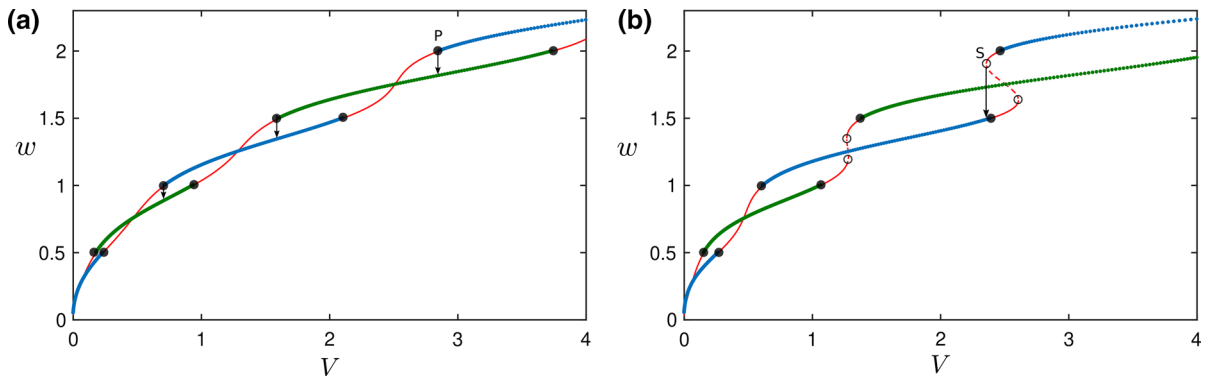

Fig. 4 Radius–volume bifurcation diagrams of a droplet resting on the extrema of the chemical pattern given as $\Theta(x) = \theta_0\,(1 + \varepsilon\cos(2\pi x))$ with $\theta_0 = \pi/3$ and $\varepsilon = 0.1$ (**a**) and $\varepsilon = 0.2$ (**b**). Blue and green lines represent stable solutions of the droplet aligned with a minimum and maximum of the chemical pattern, respectively. Red lines denote saddle-node solutions, for which the droplet is unstable to asymmetric perturbations only, and dashed lines represent fully unstable solutions. Solid circles mark the onset of pitchfork (P) bifurcations while empty circles denote saddle-node (S) bifurcations. Arrows show the change of the droplet's radius as a consequence of each bifurcation (note that, for clarity, only one arrow is plotted in panel **b**). (Color figure online)

eigenvalues. If the Hessian matrix has only positive eigenvalues then the system is stable, while if there exists a negative eigenvalue then the system is unstable.

By tracing the stable and unstable equilibrium positions as we change the volume, we are able to construct bifurcation diagrams, as shown in Fig. 4. Panel (a) shows two branches of solutions that correspond to droplets aligned with a minimum of the chemical pattern (blue curves) and a maximum (green curves). In both cases, the red regions denote solutions that are saddle nodes (i.e. they are unstable against asymmetric perturbations only). The key feature of these diagrams is the emergence of pitchfork bifurcation points at some critical volumes, which are denoted as black solid points in panel (a). Therefore, as the droplet evaporates and the volume decreases in time, the presence of asymmetric perturbations in the system can trigger lateral displacement whereby the droplet shifts from a maximum to a minimum of the chemical pattern, or vice versa (see black arrows in panel (a)). This has been referred to as snap evaporation [38]. In our model, we will assume that such transitions occur instantly.

When we increase the strength of the chemical pattern, ε, the stability diagrams show the existence of saddle-node bifurcations, which are denoted as empty circles in Fig. 4b. Under these conditions, if the system is not affected by any perturbation, it may be possible that, as the droplet evaporates along a stable branch, the droplet bypasses the pitchfork bifurcation and reaches the critical turning point of the saddle-node bifurcation. At this point there is no further solutions and the droplet radius rapidly decreases while the droplet remains at the same location. This is illustrated by the arrow in Fig. 4b.

In the following section, we use these ideas to construct the stability path of a droplet evaporating on a smooth pattern.

5 Droplet lifetimes

In this section, we investigate the lifetime of a droplet resting on a smooth patterned surface. As the droplet evaporates, it evolves according to the model described in Sect. 4, while the rate at which it evaporates is calculated from (14). We also assume that the shape of the droplet is always given by its equilibrium configuration with both contact angles equal. Hence, the droplet is assumed to evolve according to

$$\frac{\mathrm{d}V}{\mathrm{d}t} = \frac{w}{\sin\Theta(d+w)} \int_{-\Theta(d+w)}^{\Theta(d+w)} \left.\frac{\partial c}{\partial n}\right|_{(x(\phi),h(\phi))} \mathrm{d}\phi, \tag{26}$$

where at each time step, d and w correspond to an equilibrium solution for the corresponding volume. The evolution is then found by integrating (26) with the initial condition $V(t = 0) = V_0$, and it is concluded at $t = \tau$, when $V < \text{tol}$, for some small numerical tolerance, $0 < \text{tol} \ll 1$, which defines the lifetime τ of the droplet. Here, we have used $\text{tol} = 10^{-4} V_0$ but other values were considered observing no effect in the results. We shall study different wetting cases, which lead to different evaporation modes.

5.1 No patterning ($\varepsilon = 0$)

We start by considering a substrate without a patterning, i.e. $\varepsilon = 0$. In this case we are simply in the classical slip evaporation mode. The lifetime of a droplet τ is depicted in Fig. 5 as a function of the contact angle. We see that the lifetime of the droplet, away from the extremely hydrophobic case, matches the general pattern of the evaporation rate, shown in Fig. 3b. In the extremely hydrophobic region, we see that the lifetime of the droplet increases dramatically with θ to a finite value as $\theta \to \pi$. We note that this is consistent with the results reported in [22] for highly hydrophobic axisymmetric droplets, although in that case the asymptotic limit $\theta \to \pi$ is approached from above. The results presented in Fig. 5 show that the lifetime of a droplet is mostly independent of θ under partial wetting conditions, but it dramatically reduces or increases as the droplet becomes highly hydrophilic or highly hydrophobic, respectively.

We can compare these results with the lifetimes that have been predicted elsewhere under special conditions. First consider the case of the extremely hydrophilic droplet ($\theta \ll 1$) that was first detailed in [24]. In this case the volume of the droplet can be accurately approximated by $V = 2w^2\theta/3$. Hence, we obtain the differential equation (noting that θ is constant)

$$\frac{2\theta}{3}\frac{\mathrm{d}w^2}{\mathrm{d}t} = -\frac{\pi}{\operatorname{asinh}\left(\frac{R}{w}\right)}. \tag{27}$$

This differential equation can be integrated implicitly over $t \in (0, \tau)$, where τ gives the lifetime of the droplet, to yield

$$\tau = \frac{2\theta}{3\pi}\left[R\sqrt{w^2 + R^2} + w^2 \operatorname{asinh}\left(\frac{R}{w}\right) - R^2\right] \qquad \text{for } \theta \ll 1, \tag{28}$$

which agrees with the result reported in [24]. The second case of interest is when the droplet has contact angle $\pi/2$. Under these conditions we obtain the differential equation

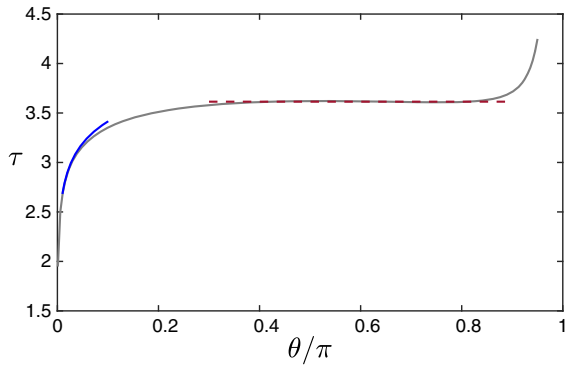

Fig. 5 The lifetime of a droplet evaporating, from an initial volume of $V_0 = 2$ on a smooth surface with no patterning depicted (i.e. $\varepsilon = 0$) as a function of the contact angle. Blue solid line and red dashed line represent the two special cases of extremely hydrophilic conditions, Eq. (28), and neutral wetting conditions, Eq. (30), respectively. (Color figure online)

$$\frac{\mathrm{d}V}{\mathrm{d}t} = -\frac{\pi}{\ln\left(\frac{R}{w}\right)}, \tag{29}$$

where $V = \pi w^2/2$. This, again, may be integrated implicitly to obtain

$$\tau = \frac{V}{2\pi}\left[1 + \ln\left(\frac{\pi R^2}{2V}\right)\right] \qquad \text{for } \theta = \frac{\pi}{2}, \tag{30}$$

which is consistent with the result obtained in [21,22,28] for axisymmetric 3D droplets, except for the dependency on the fictitious infinity R, which is not required in the 3D problem. Figure 5 shows the lifetime of the droplet as a function of the contact angle using the exact equation and the two special cases we have discussed here. We see that the exact equation matches the special cases in their respective regimes. Indeed, the small angle approximation agrees well with the exact form for contact angles less than 0.05π, and the hydroneutral solution gives a good approximation for contact angles between 0.4π and 0.8π.

5.2 Sinusoidal patterning ($\varepsilon \neq 0$)

We next consider the case with a smooth chemical pattern, $\varepsilon \neq 0$, and we will distinguish between two different modes. Firstly, consider a droplet which is unable to shift its position as it loses stability. This can be thought of as an analogue to a 3D droplet at the centre of a concentric rings patterning. In this case, the droplet will evaporate along the corresponding branch in the bifurcation diagram, but because the centre is fixed, the droplet will not snap to a new position when it loses stability (see Fig. 4b). In the second case, we allow the droplet to shift at each pitchfork bifurcation leading to lateral snaps along the droplet's position (see Fig. 4a).

Figure 6 compares the evolution of these two different cases alongside the homogeneous case ($\varepsilon = 0$). Panels (a) and (b) show the corresponding evolution of the droplet's width as a function of the volume, where we can see that when the droplet is fixed, the droplet's width follows a single bifurcation branch (see panel (a)), but when the droplet is free to traverse the surface it snaps at the pitchfork bifurcation point (see panel (b)). Panel (c) shows the

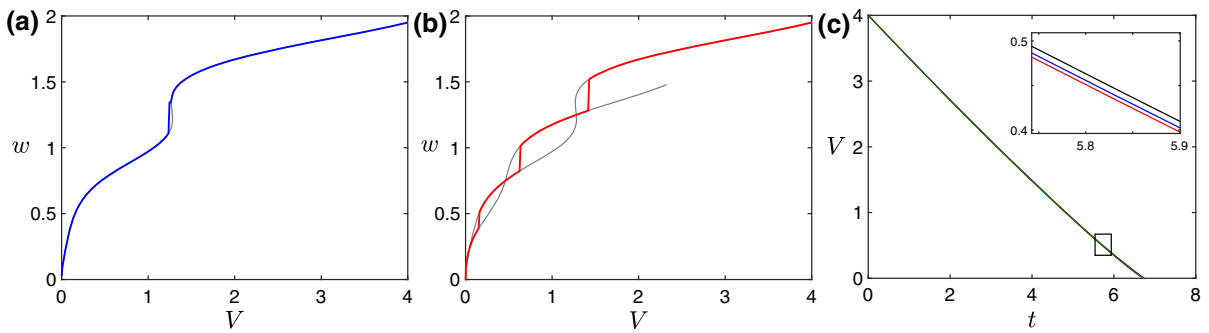

Fig. 6 **a** Droplet's width as function of the volume when the droplet remains fixed at the same location without lateral shift. The underlying grey line denotes the bifurcation diagram of equilibrium solutions from Sect. 4. **b** Droplet's width as function of the volume when the droplet is allowed to shift at each pitchfork bifurcation. The underlying grey lines show the corresponding bifurcation diagrams. In both **a** and **b** the strength of the chemical pattern is $\varepsilon = 0.2$. **c** Time evolution of the droplet's volume. The inset shows a magnified plot of the region marked with a rectangle, where the blue and red lines correspond to the cases of (a) and (b), respectively, and the black line corresponds to a homogeneous surface ($\varepsilon = 0$). In all cases the average contact angle is $\theta_0 = \pi/3$. (Color figure online)

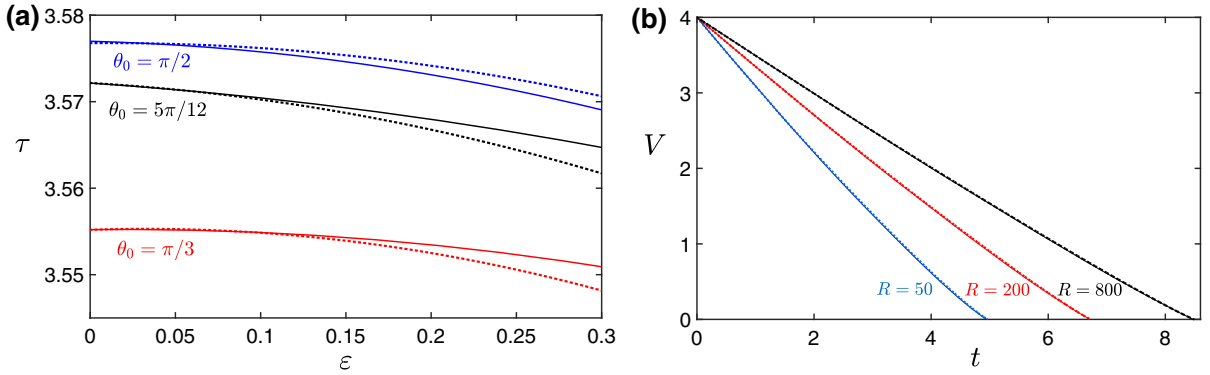

Fig. 7 **a** Droplet's lifetime as a function of the chemical pattern strength ε with average contact angle $\pi/2$ (blue), $5\pi/12$ (black), and $\pi/3$ (red). The two modes of evaporation are also shown with a fixed centre position depicted with solid lines while the dot curves represent droplets which are free to translate along the substrate. **b** Volume time evolution for different cases of the parameter R, namely $R = 50$, 200 and 800 for the blue, red and black curves, respectively. The solid/dashed lines correspond to droplets which are fixed/move freely. In all cases, the pattern parameters are $\theta_0 = \pi/3$ and $\varepsilon = 0.3$. (Color figure online)

time evolution of the volume for all cases. Interestingly, the volume of the droplet, given as a function of time, does not change significantly, and in particular, the droplet on the homogeneous surface has a marginally longer lifetime, while the freely moving droplet has a marginally shorter lifetime. This can be explained by considering Fig. 3a, in the region around $\theta = \pi/3$. We see that the evaporation rate is an increasing function around $\theta = \pi/3$. Hence, time-averaged contact angle for the droplets on the patterned surfaces must be greater than the spatially-averaged contact angle. Further, the droplet which is free to traverse the surface is able to maintain a higher contact angle for longer than the droplet which is fixed in position.

We now consider how the droplet's evolution is affected by changing ε. In Fig. 7a we compare the lifetime of the droplet under the two regimes, as a function of ε, for various θ_0. It is shown that increasing the patterning amplitude decreases the lifetime of the droplet. We also note that the difference between both regimes increases as $\varepsilon \gtrsim 0.1$, which can be attributed to the fact that above this value, there is the existence of saddle-node bifurcations that affect the dynamics of the droplet. It should be further noted that as the droplet becomes more hydrophobic (but not in the extreme region) the lifetimes drop, but follow the same trends as shown. Interestingly, there is a value of θ_0 between $\pi/2$ and $5\pi/12$ where the droplet lifetime switches from being longer for a static droplet to being longer for a freely moving droplet. We also study how the time evolution of the droplet depends on the value of the outer boundary R, which has been shown to have an effect in similar type of two-dimensional problems [24,25] . In Fig. 7b we can see that increasing R increases the lifetime of the droplet, as expected. We also compare the evolution of the droplet under the two evaporation settings, where we note that the lifetime of the droplet varies marginally between the two regimes (difference between solid and dashed lines in Fig. 7b).

6 Discussion

We have investigated the evolution and lifetime of an evaporating two-dimensional sessile droplet resting atop a smooth patterned surface. The evaporation rate was calculated following the approach introduced in [25], which was then used to obtain an asymptotic expression for the limiting case of nearly neutral wetting. We also considered the limiting case of highly hydrophilic droplets, which was in agreement with the result reported in [24].

We found that the evaporation rate of the droplet is highly dependent on the size and shape of the fictitious infinity where the far-field boundary conditions are applied. Indeed, if the ratio of the radii of the fictitious infinity and the droplet is held constant, i.e. $R = w(t) \times$ const., then the evaporation rate remains almost constant. However, it makes physical sense to hold R constant as the droplet evaporates, rather than keeping the ratio of R and w constant. This dependence on the fictitious infinity was also reported in [24].

To estimate the lifetime of the droplet, we assumed that the evolution of the droplet's radius, w, as the volume V varies is dictated by the wetting equilibrium properties. This is quantified in terms of bifurcation diagrams $w(R)$ which show the emergence of pitchfork and saddle-node bifurcations where solutions change stability [39,40]. Such hierarchy of bifurcations allows us to distinguish between two distinctive droplet's time evolution. In one case, the droplet is allowed to shift translationally at each pitchfork bifurcation, and on the other case, the location of the droplet is fixed but its width undergoes a transition at each saddle-node bifurcation. Hence, given a given chemical pattern, the time evolution of the volume is constructed by combining the information from the evaporation rate and the bifurcation diagrams.

We found that the lifetime of the droplet depends subtly on the contact angle, θ_0, the parameter ε and the droplet's evolution path. Indeed, it was shown that the lifetime of the droplet is maximised for a droplet with average contact angle $\pi/2$ and with $\varepsilon \lesssim 0.1$. This result is expected since the evaporation rate of the droplet is at its slowest for $\theta = \pi/2$, as shown in Fig. 3b, and the contact angle is at this critical value for longest with $\varepsilon = 0$. Our results also showed that the droplet's lifetime always decreases with the strength ε of the pattern, indicating that droplets evaporate faster on wetting patterns than on homogeneous surfaces. It was further found that the two evaporation scenarios predict near equal lifetimes for $\varepsilon \lesssim 0.1$ while when ε exceeds this value the two lifetimes begin to diverge. The case for which the droplet shifts laterally as it evaporates (snap evaporation) was found to have shorter lifetimes for droplets away from the nearly neutral case, whereas in the nearly neutral case, this snap mode increased the lifetime of the droplet.

It was shown that the lifetime does not change significantly as the contact angle changes (but remains away from the extreme cases), and the lifetime similarly only subtly changes with ε. The lifetime can be bound above (and approximated) by the case where the contact angle is always $\pi/2$, which yields

$$\tau \lesssim \tau_{\pi/2} = \frac{V_0}{2\pi}\left(1 + \ln\frac{\pi R^2}{2V_0}\right), \tag{31}$$

or in dimensional terms, the lifetime of the droplet, T, may be bounded by

$$T \lesssim \lambda D(c_{\text{sat}} - c_\infty)\frac{V_0}{2\pi}\left(1 + \ln\frac{\pi R^2}{2V_0}\right), \tag{32}$$

where λ, D, c_{sat} and c_∞ are the wavelength of the surface patterning, the diffusive coefficient, the saturated concentration of liquid vapour and natural concentration level in the surrounding fluid of the liquid vapour without the presence of a droplet, respectively.

The ideas presented in this work could be used to explore three-dimensional configurations, although it should be noted that unlike the two-dimensional case presented here, a three-dimensional droplet on a patterned surface does not necessarily take a simply described shape, even in the absence of gravity. This presents a significant challenge to overcome in order to calculate the evaporation rate and then apply the result to find the lifetime of the droplet. In addition, alternative patterns could be considered, e.g. sharper variations on the contact angle that would allow to study transitions from slip to pinned configurations. We intend to address these and related issues in the future studies.

Appendix A: Asymptotic solution to (7a)–(7d) in the nearly neutral wetting regime

As discussed in the main body of the text, the shape of the droplet's surface is described, in polar coordinates (r, ϕ), by

$$r = w(1 + \varepsilon \sin\varphi) + \mathcal{O}(\varepsilon^2), \tag{33}$$

where the small parameter ε is defined as $\varepsilon = \theta - \pi/2$ and observe $|\varepsilon| \ll 1$. To seek solutions to the Laplace system (7a)–(7d), we assume a regular asymptotic expansion for the concentration, i.e.

$$c = c_0 + \varepsilon c_1 + \mathcal{O}(\varepsilon^2). \tag{34}$$

Application of this expansion yields the leading order system

$$\left.\begin{aligned} &\frac{1}{r}\frac{\partial}{\partial r}\left(r\frac{\partial c_0}{\partial r}\right) + \frac{1}{r^2}\frac{\partial^2 c_0}{\partial \varphi^2} = 0, \\ &c_0 = 1 \ \text{ on } r = w, \\ &c_0 = 0 \ \text{ on } r = R, \\ &\frac{\partial c_0}{\partial \varphi} = 0 \ \text{ on } \varphi = 0, \pi, \end{aligned}\right\} \tag{35}$$

and the first-order system

$$\left.\begin{aligned} &\frac{1}{r}\frac{\partial}{\partial r}\left(r\frac{\partial c_1}{\partial r}\right) + \frac{1}{r^2}\frac{\partial^2 c_1}{\partial \varphi^2} = 0, \\ &c_1 = -w\sin\varphi\frac{\partial c_0}{\partial r} \ \text{ on } r = w, \\ &c_1 = 0 \ \text{ on } r = R, \\ &\frac{\partial c_1}{\partial \varphi} = 0 \ \text{ on } \varphi = 0, \pi. \end{aligned}\right\} \tag{36}$$

Solutions for the leading order system are straightforward to find and can be written as

$$c_0 = 1 - \frac{\ln\frac{r}{w}}{\ln\frac{R}{w}}. \tag{37}$$

To solve the first-order system, we seek solutions which are separable, i.e. $c_1(r, \varphi) = \rho(r) f(\varphi)$. Seeking separable solutions, we find that the two functions, $\rho(r)$ and $f(\varphi)$, must satisfy

$$r\frac{\mathrm{d}}{\mathrm{d}r}\left(r\frac{\mathrm{d}\rho}{\mathrm{d}r}\right) - k^2\rho = 0, \tag{38}$$

$$\rho(R) = 0, \tag{39}$$

and

$$\frac{\mathrm{d}^2 f}{\mathrm{d}\varphi^2} + k^2 f = 0, \tag{40}$$

$$\left.\frac{\mathrm{d}f}{\mathrm{d}\varphi}\right|_{\varphi=0,\pi} = 0, \tag{41}$$

where k is a real constant. We see that the non-homogeneous boundary condition on $r = w$ has been neglected from this system and shall be applied later. By solving these ordinary differential equations, we find

$$c_1(r,\varphi) = A_0\left(1 - \frac{\ln\frac{r}{w}}{\ln\frac{R}{w}}\right) + \sum_{k=1}^{\infty} A_k\left[\left(\frac{r}{R}\right)^k - \left(\frac{R}{r}\right)^k\right]\cos(k\varphi), \tag{42}$$

where $A_0, A_1, A_2, \ldots$ are constants, which are fixed by applying the condition on $r = w$. This condition becomes

$$A_0 + \sum_{k=1}^{\infty} A_k\left[\left(\frac{w}{R}\right)^k - \left(\frac{R}{w}\right)^k\right]\cos(k\varphi) = \frac{\sin\varphi}{\ln\frac{R}{w}}. \tag{43}$$

To then calculate $A_0, A_1, A_2, \ldots$, we multiply this condition by $\cos(m\phi)$ for $m = 0, 1, 2, \ldots$ and integrate the resulting system over $\varphi \in (0, \pi)$. This yields

$$A_0 = \frac{2}{\pi\ln\frac{R}{w}}, \quad A_{2k-1} = 0, \quad A_{2k} = \frac{4}{1-4k^2}\frac{1}{\pi\ln\frac{R}{w}}\left[\left(\frac{w}{R}\right)^{2k} - \left(\frac{R}{w}\right)^{2k}\right]^{-1}. \tag{44}$$

By combining these results, we obtain the desired result

$$c = 1 - \frac{\ln\frac{r}{w}}{\ln\frac{R}{w}} + \varepsilon\left[\frac{2}{\pi\ln\frac{R}{w}}\left(1 - \frac{\ln\frac{r}{w}}{\ln\frac{R}{w}}\right) + \frac{4}{\pi\ln\frac{R}{w}}\sum_{n=1}^{\infty}\frac{\cos(2n\varphi)}{1-4n^2}\frac{\left(\frac{r}{R}\right)^{2n} - \left(\frac{R}{r}\right)^{2n}}{\left(\frac{w}{R}\right)^{2n} - \left(\frac{R}{w}\right)^{2n}}\right] + \mathcal{O}(\varepsilon^2). \tag{45}$$

References

1. Vellingiri R, Savva N, Kalliadasis S (2011) Droplet spreading on chemically heterogeneous substrates. Phys Rev E 84:036305
2. Varagnolo S, Schiocchet V, Ferraro D, Pierno M, Mistura G, Sbragaglia M, Gupta A, Amati G (2014) Tuning drop motion by chemical patterning of surfaces. Langmuir 30(9):2401–2409
3. Honisch C, Lin T-S, Heuer A, Thiele U, Gurevich SV (2015) Instabilities of layers of deposited molecules on chemically stripe patterned substrates: ridges versus drops. Langmuir 31(38):10618–10631
4. Savva N, Groves D, Kalliadasis S (2019) Droplet dynamics on chemically heterogeneous substrates. J Fluid Mech 859:321–361
5. Liu W, Witelski TP (2020) Steady states of thin film droplets on chemically heterogeneous substrates. IMA J Appl Math 85(6):980–1020
6. Yatsyshin P, Kalliadasis S (2021) Surface nanodrops and nanobubbles: a classical density functional theory study. J Fluid Mech 913:A45
7. Picknett RG, Bexon R (1977) The evaporation of sessile or pendant drops in still air. J Colloid Interface Sci 61(2):336–350
8. Hu H, Larson RG (2002) Evaporation of a sessile droplet on a substrate. J Phys Chem B 106(6):1334–1344
9. Larson RG (2014) Transport and deposition patterns in drying sessile droplets. AIChE J 60:1538–1571
10. Brutin D, Starov V (2018) Recent advances in droplet wetting and evaporation. Chem Soc Rev 47(2):558–585
11. Zang D, Tarafdar S, Tarasevich YY, Choudhury MD, Dutta T (2019) Evaporation of a Droplet: from physics to applications. Phys Rep 804:1–56
12. Leenaars AFM, Huethorst JAM, Van Oekel JJ (1990) Marangoni drying: a new extremely clean drying process. Langmuir 6(11):1701–1703
13. Kamyshny A, Ben-Moshe M, Aviezer S, Magdassi S (2005) Ink-jet printing of metallic nanoparticles and microemulsions. Macromol Rapid Commun 26(4):281–288
14. Pajor-Świerzy A, Socha R, Pawłowski R, Warszyński P, Szczepanowicz K (2019) Application of metallic inks based on nickel-silver core-shell nanoparticles for fabrication of conductive films. Nanotechnology 30(22):225301
15. Giorgiutti-Dauphine F, Pauchard L (2018) Drying drops containing solutes: from hydrodynamical to mechanical instabilities. Eur Phys J E Soft Matter 41(3):32

16. Yang X, Jiang Z, Lyu P, Ding Z, Man X (2021) Deposition pattern of drying droplets. Commun Theor Phys 73:047601
17. Jackson JD (1998) Classical electrodynamics. Wiley, New York
18. Spiegelman M (1993) Flow in deformable porous media. Part 1 Simple analysis. J Fluid Mech 247:17–38
19. Laghezza G, Dietrich E, Yeomans JM, Ledesma-Aguilar R, Kooij ES, Zandvliet HJW, Lohse D (2016) Collective and convective effects compete in patterns of dissolving surface droplets. Soft Matter 12(26):5787–5796
20. Guerin MS, Lauga E (2018) Collective dissolution of microbubbles. Phys Rev E 3(4):043601
21. Stauber JM, Wilson SK, Duffy BR, Sefiane K (2014) On the lifetimes of evaporating droplets. J Fluid Mech 744:R2
22. Stauber JM, Wilson SK, Duffy BR, Sefiane K (2015) Evaporation of droplets on strongly hydrophobic substrates. Langmuir 31(12): 3653–3660
23. Baines WD, James DF (1994) Evaporation of a droplet on a surface. Ind. Eng. Chem. Res. 33(2):411–416
24. Schofield FGH, Wray AW, Pritchard D, Wilson SK (2020) The shielding effect extends the lifetimes of two-dimensional sessile droplets. J Eng Math 120(1):89–110
25. Yarin AL, Szczech JB, Megaridis CM, Zhang J, Gamota DR (2006) Lines of dense nanoparticle colloidal suspensions evaporating on a flat surface: formation of non-uniform dried deposits. J Colloid Interface Sci 294(2):343–354
26. Shanahan MER (1995) Simple theory of "stick-slip" wetting hysteresis. Langmuir 11(3):1041–1043
27. Orejon D, Sefiane K, Shanahan MER (2011) Stick-slip of evaporating droplets: substrate hydrophobicity and nanoparticle concentration. Langmuir 27(21):12834–12843
28. Stauber JM, Wilson SK, Duffy BR, Sefiane K (2015) On the lifetimes of evaporating droplets with related initial and receding contact angles. Phys Fluids 27(12):122101
29. Dietrich E, Kooij ES, Zhang X, Zandvliet HJW, Lohse D (2016) Stick-jump mode in surface droplet dissolution. Langmuir 31:4696–4703
30. Askounis A, Orejon D, Koutsos V, Sefiane K, Shanahan MER (2011) Nanoparticle deposits near the contact line of pinned volatile droplets: size and shape revealed by atomic force microscopy. Soft Matter 7:4152–4155
31. Schofield FGH, Wilson SK, Pritchard D, Sefiane K (2018) The lifetimes of evaporating sessile droplets are significantly extended by strong thermal effects. J Fluid Mech 851:231–244
32. Wong T-S, Kang SH, Tang SKY, Smythe EJ, Hatton BD, Grinthal A, Aizenberg J (2011) Bioinspired self-repairing slippery surfaces with pressure-stable omniphobicity. Nature 477(7365):443–447
33. Smith JD, Dhiman R, Anand S, Reza-Garduno E, Cohen RE, McKinley GH, Varanasi KK (2013) Droplet mobility on lubricant-impregnated surfaces. Soft Matter 9(6):1772–1780
34. Guan JH, Wells GG, Xu B, McHale G, Wood D, Martin J, Stuart-Cole S (2015) Evaporation of sessile droplets on slippery liquid-infused porous surfaces (slips). Langmuir 31(43):11781–11789
35. Armstrong S, McHale G, Ledesma-Aguilar R, Wells GG (2019) Pinning-free evaporation of sessile droplets of water from solid surfaces. Langmuir 35(8):2989–2996
36. Salludah MS, Launay G, Parle J, Ledesma-Aguilar R, Gizaw Y, McHale G, Wells GG (2020) Bidirectional motion of droplets on gradient liquid infused surfaces. Commun. Phys. 3:166
37. Quéré D (2005) Non-sticking drops. Rep Prog Phys 68(11):2495
38. Wells GG, Ruiz-Gutiérrez É, Le Lirzin Y, Nourry A, Orme BV, Pradas M, Ledesma-Aguilar R (2018) Snap evaporation of droplets on smooth topographies. Nat Commun 9:1380
39. Ewetola M, Ledesma-Aguilar R, Pradas M (2021) Control of droplet evaporation on smooth chemical patterns. Phys Rev Fluids 6(3):033904
40. Pradas M, Savva N, Benziger JB, Kevrekidis IG, Kalliadasis S (2016) Dynamics of fattening and thinning 2D sessile droplets. Langmuir 32(19):4736–4745
41. Wray AW, Duffy BR, Wilson SK (2020) Competitive evaporation of multiple sessile droplets. J Fluid Mech 884:A45